aerospace

MDPI

Article

Dynamic Numerical Simulation of Hybrid Rocket Motor with HTPB-Based Fuel with 58% Aluminum Additives

Hui Tian [1,2], Xiangyu Meng [1,2], Hao Zhu [1,2,*], Chengen Li [3], Lingfei He [1,2] and Guobiao Cai [1,2]

1 School of Astronautics, Beihang University, Beijing 100191, China
2 Key Laboratory of Spacecraft Design Optimization & Dynamic Simulation Technologies, Ministry of Education, Beijing 100816, China
3 Science and Technology on Space Physics Laboratory, China Academy of Launch Vehicle Technology, Beijing 100076, China
* Correspondence: zhuhao@buaa.edu.cn

Abstract: The addition of aluminum (Al) to the fuel is an effective way to increase the regression rate of hybrid rocket motors (HRMs). Due to its high regression rate, the impact of the regression of combustion surface on the performance of HRMs cannot be ignored. Therefore, it is significant to establish a dynamic numerical simulation model to predict the performance of HRMs. In this study, the dynamic simulation model was established based on dynamic mesh technology and was verified by a firing test. The results show that the simulation results agree well with the experimental results, and the errors of the average thrust and combustion chamber pressure are 3.4% and 1.4%, respectively. The dynamic simulation shows that with the regression of the combustion surface, the vortex of the pre-combustion chamber is divided into two vortices. The vortex near the front of the grain will increase the regression rate downstream. The results show that the addition of Al can obviously improve the regression rate of HRMs. The fuel containing 58% Al can improve the regression rate by 88.8% compared with the fuel with pure hydroxyl-terminated polybutadiene (HTPB). Moreover, due to the higher combustion temperature and the scouring of metal particles, the ablation rate of the nozzle with carbon ceramic materials reaches 0.16 mm/s. This investigation provides a valuable reference for HRMs design and simulation.

Keywords: hybrid rocket motor; dynamic numerical simulation; Al-containing fuel; regression rate

Citation: Tian, H.; Meng, X.; Zhu, H.; Li, C.; He, L.; Cai, G. Dynamic Numerical Simulation of Hybrid Rocket Motor with HTPB-Based Fuel with 58% Aluminum Additives. *Aerospace* **2022**, *9*, 727. https://doi.org/10.3390/aerospace9110727

Academic Editor: Stephen Whitmore

Received: 8 October 2022
Accepted: 18 November 2022
Published: 18 November 2022

1. Introduction

Typical hybrid rocket motors (HRMs) propellants consist of solid fuel and liquid oxidizers [1–4]. Since the propellants are stored in different phases, respectively, the hybrid rocket motor has obvious advantages compared with solid and liquid rocket motors in terms of simple structure, adjustable thrust, high safety, low cost, and multiple restart capabilities [5–8]. The advantages make it suitable for missile systems, attitude control motors, small launch vehicles, and space tourism. The prospect of the hybrid rocket motor is extremely broad [9–13].

Hydroxy-terminated polybutadiene (HTPB) is one of the commonly used solid fuels for HRMs. However, due to the characteristic of low regression rate, additives with high energy are commonly used to increase the regression rate. Due to high heat and density, aluminum (Al) is a widely investigated additive in HRMs. George et al. [14] have conducted many ground firing tests of the Al-containing fuel. The results demonstrate that the addition of Al has an effect of enhancement on the regression rate in the hybrid rocket motors. Sun et al. [15] carried out several ground firing tests, which demonstrate that the addition of 10% Magnesium (Mg), 28% Al, and 2% Carbon (C) resulted in a 12% increase in the regression rate of the pure HTPB. Sun et al. [16] also demonstrated through steady-state simulations and experiments that the regression rate increased significantly with the increase of Al content, however, there is no significant relationship between the regression rate and the diameter of Al particles, which agrees well with the experimental results carried out by Strand et al. [17]. In addition, according to ref. [16], the Al particle diameter has a great influence on the vacuum specific impulse and characteristic velocity. The vacuum specific impulse and characteristic velocity decrease with the increase of the Al particle diameter.

To the best of the authors' knowledge, there are few dynamic simulation studies on the effect of Al on the performance of HRMs. In this paper, 95% hydrogen peroxide (95HP) was adopted as the liquid oxidizer of HRMs, and the numerical simulation was carried out by ANSYS Fluent 2022 R1 software. The realizable k-ε turbulence model, fuel pyrolysis model, finite-rate chemical reaction models, and dynamic mesh technology were used to establish the dynamic numerical simulation model of HRMs. The effect of 58% Al on the performance of HRMs such as regression rate, thrust, and pressure is obtained. In addition, ground firing tests were conducted to verify the accuracy of the simulation model based on the 100 mm diameter HRMs test platform. The results show that the addition of Al can significantly improve the regression rate of HRMs, and the model provides a valuable reference for design and optimization.

2. Dynamic Simulation Models

The combustion model of hybrid rocket motors is typical of diffusion combustion. Therefore, reasonable assumptions for the combustion model are shown as follows:

- Gas phase component is considered to be ideal gas;
- In the inner flow field, only the gas-phase reaction is considered;
- The flow and combustion are supposed to be axisymmetric.

2.1. Transient Governing Equation

The governing equations of hybrid rocket motors are shown as follows [5]:

$$\frac{\partial \rho \Phi}{\partial t} + \frac{\partial(\rho u \Phi)}{\partial x} + \frac{1}{r}\frac{\partial(r \rho v \Phi)}{\partial r} = \frac{\partial}{\partial x}\left(\Gamma \frac{\partial \Phi}{\partial x}\right) + \frac{1}{r}\frac{\partial}{\partial r}\left(r \Gamma \frac{\partial \Phi}{\partial r}\right) + S_\Phi \tag{1}$$

where Φ is the general variable, S_Φ refers to the source item, Γ denotes the diffusion coefficient. t refers to the time, x denotes the axial coordinates, ρ refers to the density, u represents the axial velocities, v refers to the radial velocities, and r represents the radial coordinates.

2.2. Gas–Solid Coupled Model

Grain surfaces maintain the conservation of mass and conservation of energy [18], as shown in:

$$\rho_g u = -\rho_f \dot{r} \tag{2}$$

$$-\lambda_g \left(\frac{\partial T}{\partial r}\right)_g = \rho_f \dot{r}\left(h_g - h_s\right) \tag{3}$$

where λ_g refers to the thermal conductivity, h_g is the enthalpy of pyrolysis products, h_s refers to the enthalpy of fuel, ρ_g is the density of pyrolysis products, and ρ_f refers to the density of fuel, $\dot{r}$ refers to the regression rate.

2.3. Turbulent Model and Chemical Reaction Model

In this investigation, the realizable k-ε turbulent model is adopted, and the enhanced wall treatment is employed for near-wall modeling. The finite-rate model is used as the reaction model. To obtain the highest density specific impulse, different ratios of HTPB and Al for the fuel were analyzed theoretically using Rocket Propulsion Analysis (RPA) [19] software by keeping the oxidizer of 95HP as constant. It is found that the density-specific impulse of the fuel with 42%HTPB + 58%Al is highest within the ratio of oxidizer to fuel of 1–6, as shown in Figure 1. Therefore, the fuel with 42%HTPB + 58%Al was adopted in this hybrid rocket motor. In addition, the Al particle diameter is 2 μm. The HTPB is assumed to be completely decomposed to C_4H_6. The chemical mechanism adopted in this simulation, which has 9 components and 13 reactions [20], is represented in Table 1. The Al chemical reaction is also shown in Table 1. Where A_1 is the constant in the chemical model, E refers to the chemical activation energy, R is the molar gas constant, and B is the constant in the chemical model.

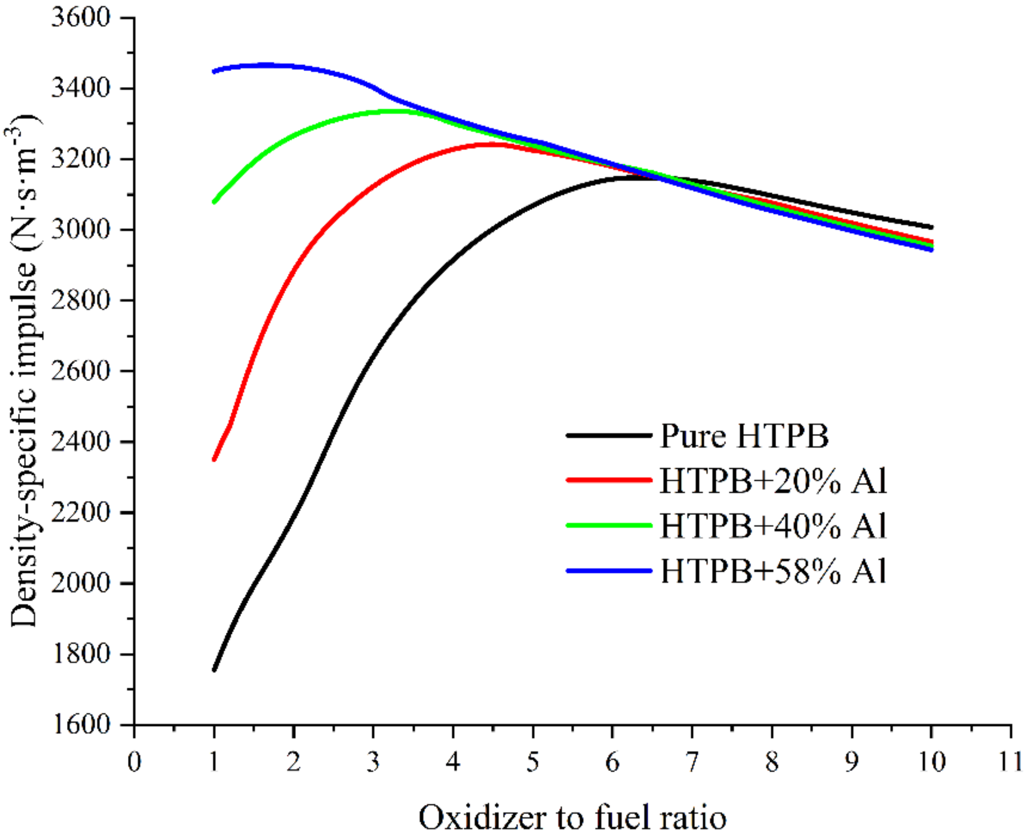

Figure 1. Density-specific impulse changes with the ratio of oxidizer to fuel.

Table 1. The chemical reaction mechanism of HRMs.

Reaction Serial Number	Reaction Equation	A_1	B	E/R (K)
1	$C_4H_6 + 2O_2 \rightleftharpoons 4CO + 3H_2$	8.80×10^{11}	0.0	15,200
2	$H_2 + O_2 \rightleftharpoons 2OH$	1.70×10^{13}	0.0	24,100
3	$OH + H_2 \rightleftharpoons H_2O + H$	2.19×10^{13}	0.0	2590
4	$2OH \rightleftharpoons O + H_2O$	6.02×10^{12}	0.0	550
5	$O + H_2 \rightleftharpoons OH + H$	1.80×10^{10}	1.0	4480
6	$H + O_2 \rightleftharpoons OH + O$	1.22×10^{17}	−0.91	8370
7	$H + O + M \rightleftharpoons OH + M$	1.00×10^{16}	0.0	0
8	$O + O + M \rightleftharpoons O_2 + M$	2.55×10^{18}	−1.0	59,400
9	$H + H + M \rightleftharpoons H_2 + M$	5.00×10^{15}	0.0	0
10	$H + OH + M \rightleftharpoons H_2O + M$	8.40×10^{21}	−2.0	0
11	$CO + OH \rightleftharpoons CO_2 + H$	4.00×10^{12}	0.0	4030
12	$CO + O_2 \rightleftharpoons CO_2 + O$	3.00×10^{12}	0.0	25,000
13	$CO + O + M \rightleftharpoons CO + M$	6.00×10^{13}	0.0	0
14	$2Al + 1.5O_2 \rightleftharpoons Al_2O_3$	9.70×10^{13}	0.0	9600

2.4. Fuel Pyrolysis Model

In this investigation, Arrhenius formula is usually used to calculate the regression rate, as shown in [21]:

$$\dot{r} = A\exp(-E_a/RT_s) \tag{4}$$

where T_s represents the temperature of the grain surface. A denotes the pre-exponential constant. In this project, when $T_s > 722$ K, A = 11.04 mm/s, E_a = 20.5 kJ/mol; when $T_s \leq 722$ K, A = 3965 mm/s, E_a = 55.8 kJ/mol [21].

2.5. Motor Computational Mesh

A two-dimensional motor computational mesh is established, as shown in Figure 2. The mesh height of the first layer is 0.01 mm, guaranteeing the calculation accuracy of the boundary layer. The elements adopt a quadrilateral structure away from the grain surface to improve the calculation speed. The wall Y^+ value is 0.33, and the total number of mesh elements is 42,392 before starting the dynamic simulation. The grid convergence test is conducted in the steady-state simulation, as shown in Figure 3. It is noticed that when the total number of mesh elements is more than 42,392, the average regression rate basically does not change with the grids number. The boundary condition between the structured grids and the unstructured adopts interface. The structure sizes of this HRM are shown in Table 2.

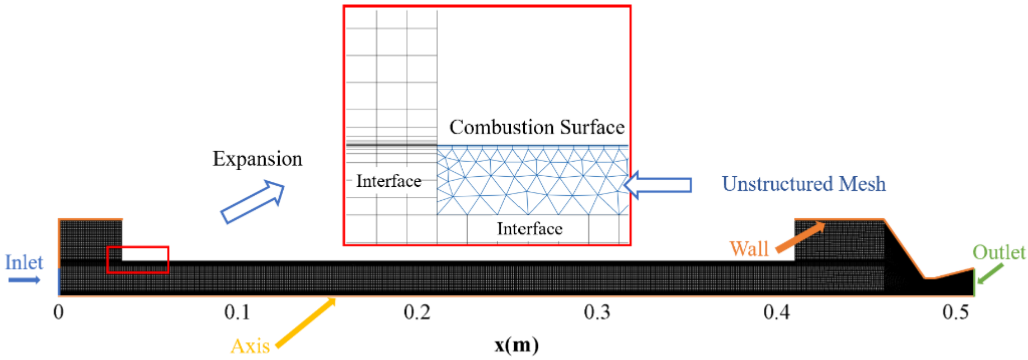

Figure 2. Computational mesh of this HRM.

Table 2. Structure sizes of this motor.

Parameter	Size (mm)
Outlet diameter of combustion chamber	100
Inner diameter of combustion chamber	80
Length of Pre-chamber	35
Length of grain	375
Length of Post-chamber	50
Grain inner diameter	35
Nozzle throat diameter	15
Nozzle outlet diameter	26
Nozzle convergence length	21.6
Nozzle divergence length	12.8

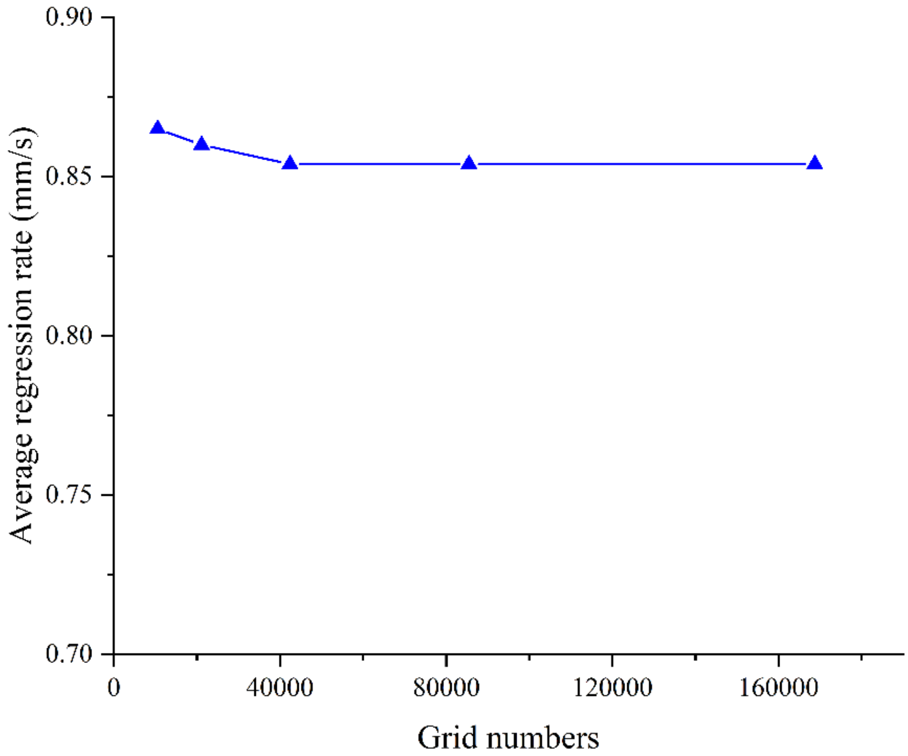

Figure 3. Average regression rate at different grid numbers.

2.6. Dynamic Mesh Technology

Dynamic mesh technology was adopted to simulate the motion boundary of the grain surface. Figure 4 shows the dynamic mesh update process. The moving distance of each node is controlled by regression rate and time. Two update meshes methods are coupled in the simulation. The methods are spring smoothing method and remeshing method. In addition, the simulation adopts the single-core calculation in the computer to avoid computing errors.

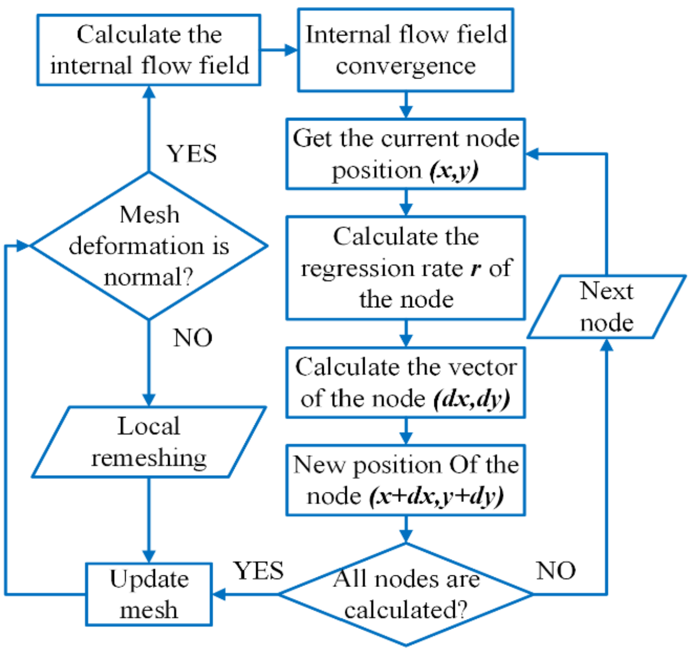

Figure 4. Dynamic mesh update process.

2.7. Boundary Conditions

It is assumed that hydrogen peroxide has been completely decomposed at the outlet of the catalytic bed, which is also the pre-chamber inlet in the simulation. The oxidizer inlet condition is a mixture of 42.35% oxygen and 57.65% water, and the mixture temperature is 1120 K. The catalytic bed uses silver as the main catalyst, which will cause a catalytic decomposition reaction of 95HP and release a lot of heat. The temperature of the catalytic decomposition products can reach 1120 K, which can provide the heat for ignition. According to our previous tests, the catalytic bed decomposition efficiency is greater than 98%, so the assumption is acceptable. The mass flow rate of oxidizer is 160 g/s. In addition, the pressure of the nozzle outlet is 101.325 KPa. Adiabatic wall condition and no-slip velocity condition are adopted at the surface of the walls. The temperature boundary calculated by the user-defined function is used for the grain surface in ANSYS Fluent 2022 R1. The temperature boundary and regression rate calculation process are shown in Figure 5. Equations (3) and (4) are coupled to calculate the temperature boundary and regression rate.

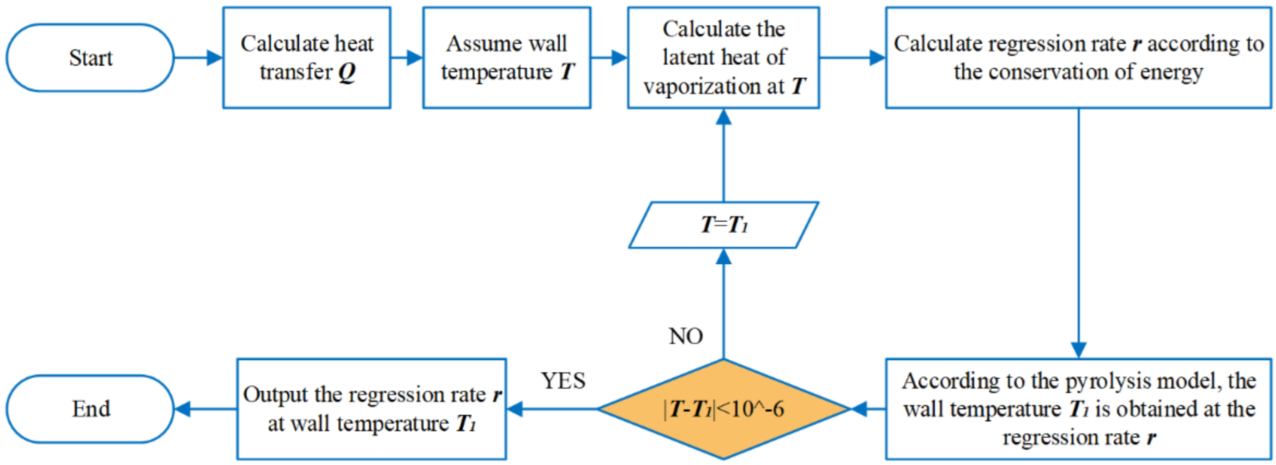

Figure 5. The temperature boundary and regression rate calculation process.

The coupled scheme was adopted in the solution methods. The spatial discretization of the second order is used for pressure, the second order upwind is used for density and energy, and the first order upwind for turbulent equations. In order to ensure the solution accuracy, the time step is 0.001 s. Moreover, the convergence criteria are used as follows: (1) the deviation of mass flow rate between the inlet and the outlet is less than 10^{-6} kg/s; (2) the residuals of main parameters are less than 10^{-3}.

3. Ground Experimental Setup

3.1. Rocket Motor

The ground firing test was conducted with a 100 mm diameter HRM. Figure 6 shows the schematic of this HRM, which consists of a catalytic bed, a combustion chamber, and a nozzle. The catalytic bed is used to achieve ignition. The nozzle of this HRM adopted carbon-ceramic as throat insert material is a Laval nozzle, which used a conical shape. Figure 7 shows the picture of this HRM.

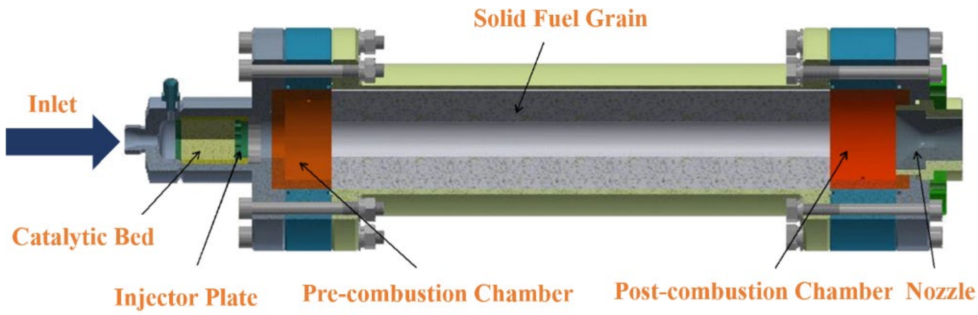

Figure 6. Schematic of experimental HRM [4].

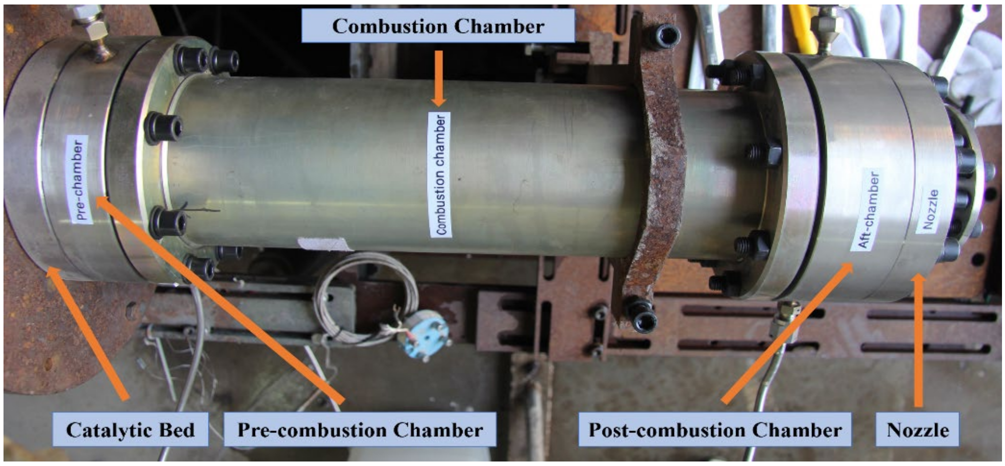

Figure 7. Picture of this HRM.

3.2. Feed System of Hydrogen Peroxide

The oxidizer feeding system of the firing test uses the extrusion oxidizer feed system. The system mainly consists of gas regulators, H_2O_2 tank, flowmeter, valves, and adjustable venturi. The oxidizer feed system of the ground experiment is shown in Figure 8. The valves and venturi are controlled by PLC. The pressure and thrust sensors are adopted in this system. The thrust sensor is an S-shaped pull/pressure sensor within ±1.5 kN. The error of thrust sensor is less than 0.5%. The sputtered thin film pressure sensor is used to measure the pressure within 0–10 MPa. The error of pressure sensor is less than 0.2%. The venturi was adopted to adjust the mass flow rate.

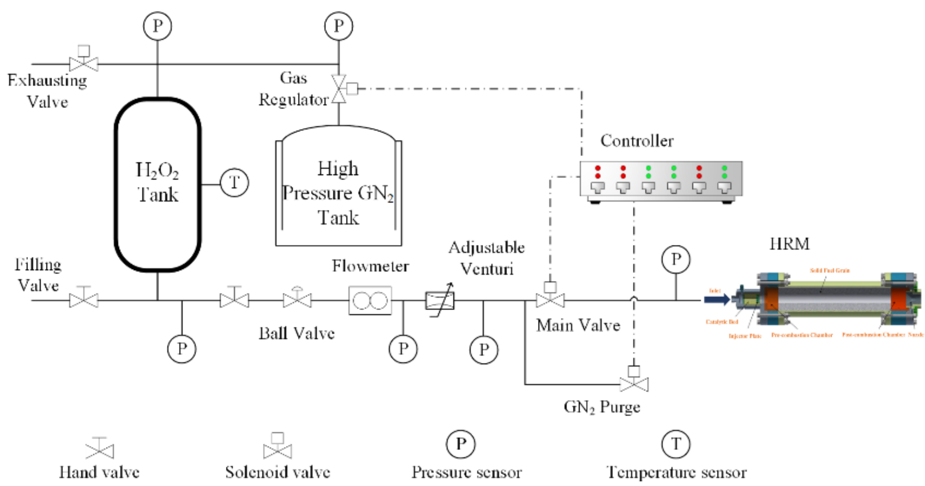

Figure 8. Feed system of hydrogen peroxide.

4. Results and Discussions

4.1. Simulated Analysis of Inner Flow Field

The mesh of the pre-combustion chamber and the front of the grain is shown in Figure 9. From the initial moment, the combustion surface is continuously receding, and the regression rate of the front of the grain is obviously higher than the regression rate of the position downstream, which is consistent with the theoretical analysis and test results. This is due to the Blasius effect, in which the boundary layer thickness at the front of the fuel grain is very thin and the heat transfer is very strong, therefore, the regression rate is high. As the thickness of the boundary layer increases along the axial distance, the heat transfer decreases. However, since the addition of fuel along the axial distance, the trend is weakened. The results demonstrate that the use of dynamic mesh technology to simulate the combustion surface regression of HRMs has obvious advantages and can well-simulate the motor operation process.

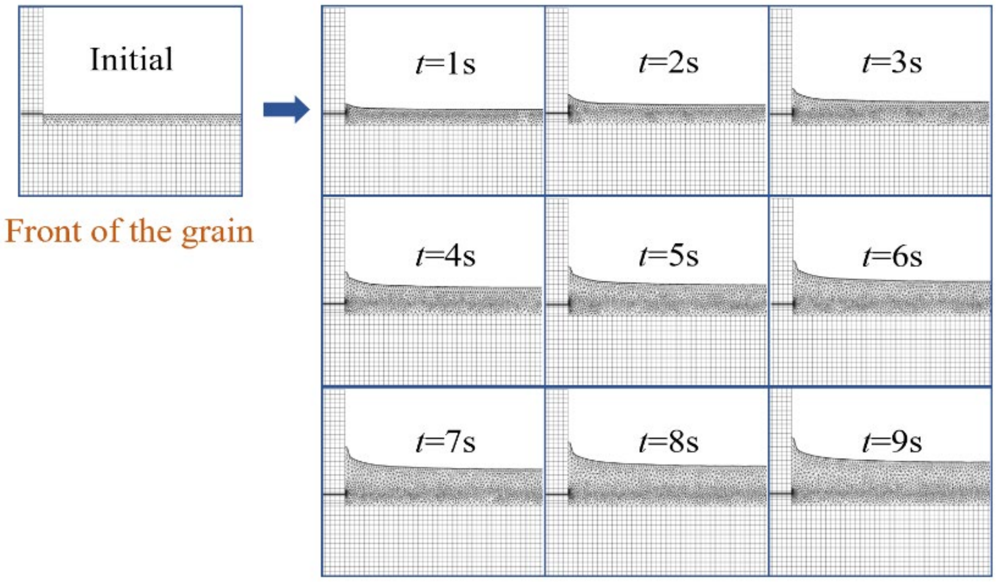

Figure 9. Mesh of the pre-chamber and the front of grain.

Further analysis of the temperature contour and streamline with time shows that an obvious flame layer occurs in the inner flow field of the combustion chamber in HRM, as shown in Figure 10. The reason is that the combustion model of the hybrid rocket motor is the typical non-premixed diffusion combustion. The temperature contour of the pre-chamber is shown in Figure 11. It was found that the average temperature increases first and then decreases. The average temperature of the pre-chamber is shown in Figure 12. At 0–4 s, the average temperature increases rapidly, with a range of 1140.8–2690.5 K. The main reason is that the pre-chamber vortex carried more fuel into the pre-chamber and enhanced diffusion combustion, resulting in a high temperature of the pre-chamber gas. At 4–5 s, the changes of the average temperature in the pre-chamber are very small. After 5 s, the average temperature of the pre-chamber gradually decreases, with a range of 2667.0–2529.0 K. The main reason is that the pre-chamber vortex splits into the pre-chamber vortex and the front vortex of the grain, as shown in Figures 10 and 11. The front vortex of the grain moves back with time, so the vortex area within the pre-chamber decreases. The temperature of the front vortex of the grain is higher than the pre-chamber vortex. Therefore, the average temperature of the pre-chamber gradually decreases.

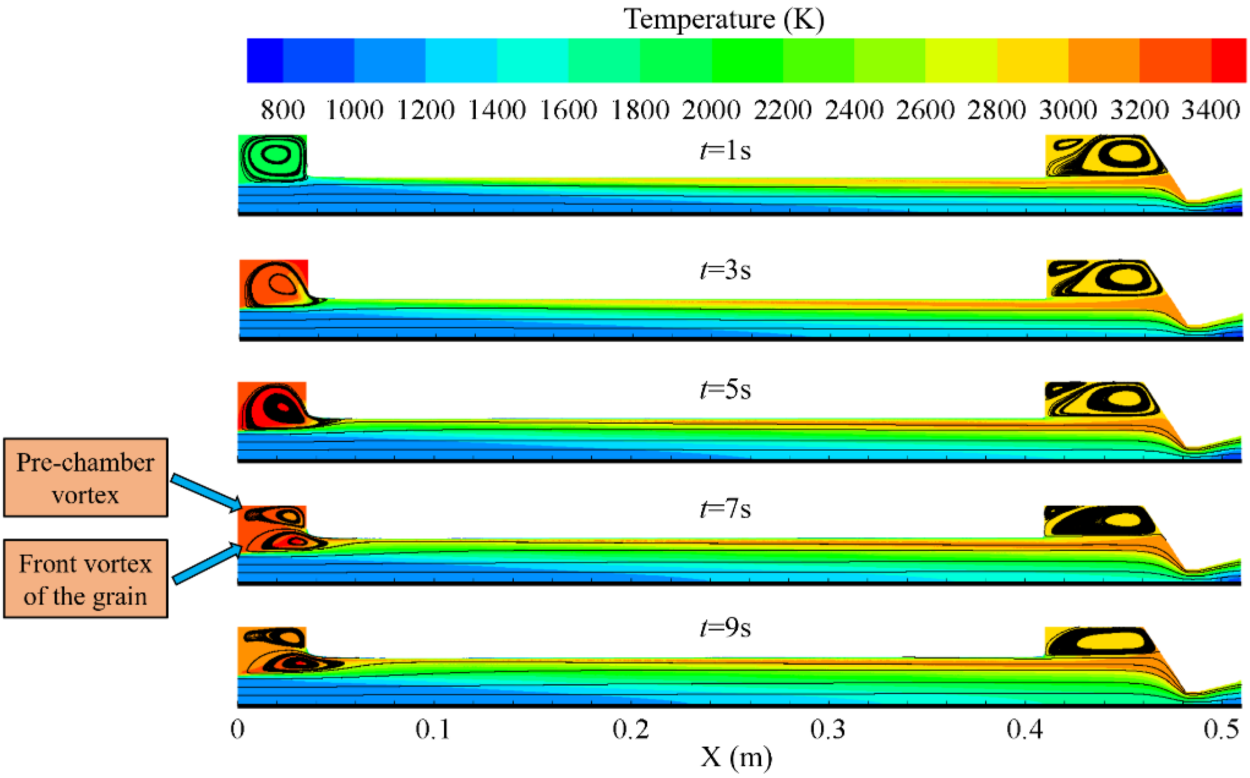

Figure 10. Temperature contour and streamline with time.

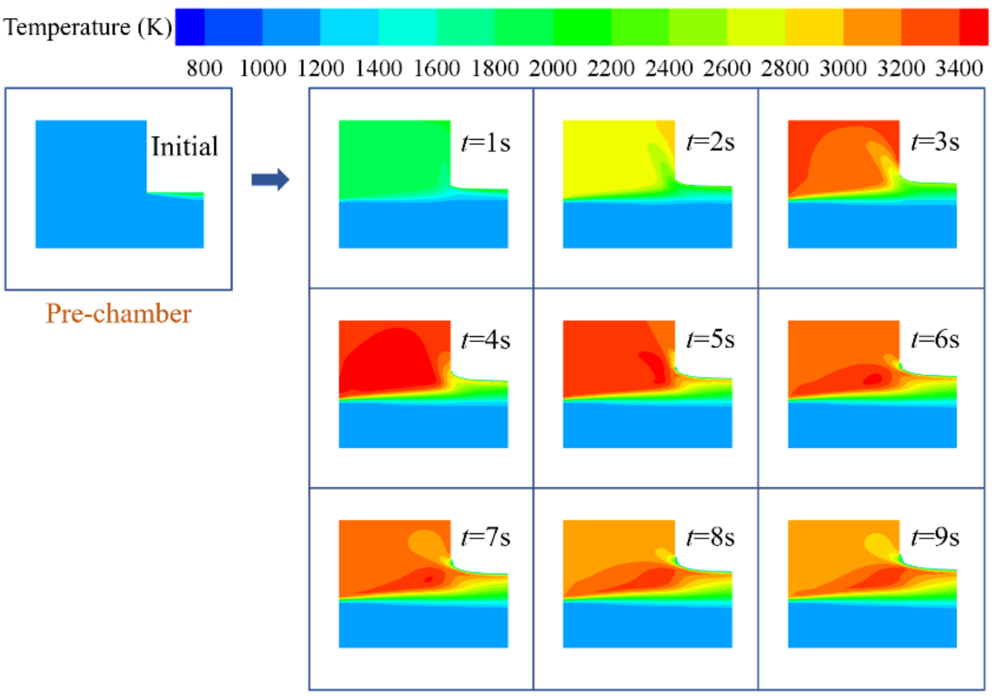

Figure 11. Temperature contour of the pre-chamber.

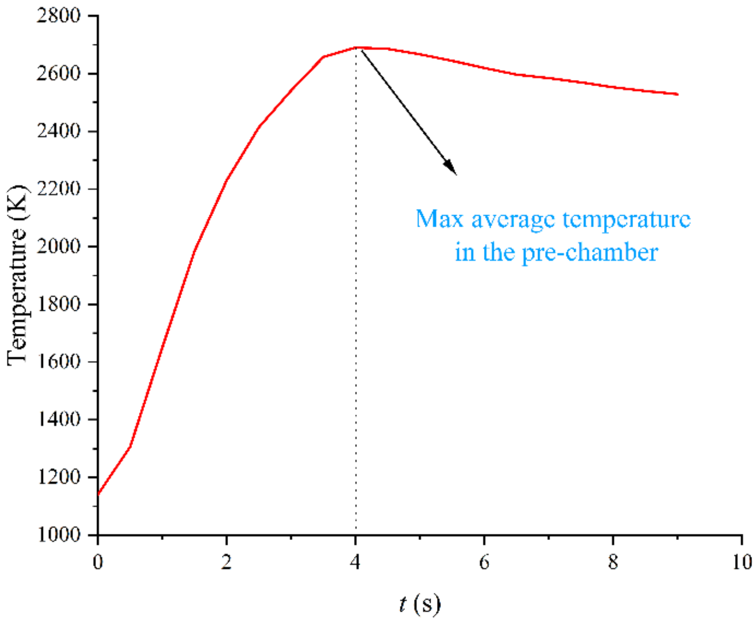

Figure 12. The average temperature of the pre-chamber varies with time.

The reason for vortex splitting is the regression of combustion surface. The regression of the combustion surface causes the pre-chamber vortex to move back, at 0–5 s. Then the pre-chamber vortex will split into the pre-chamber vortex and the front vortex of the grain. The gas temperature of the post-chamber is about 3000 K during the operation process. Since the regression of the combustion surface, the size of the backflow zone of the post-chamber decreases gradually. Therefore, the size of the vortex in the post-chamber decreases gradually.

The four species with the highest mass fraction were selected as follows: H_2O, Al_2O_3, O_2, C_4H_6. At the initial moment (t = 0 s), the mass fraction of four species within the inner flow field of HRMs is represented in Figure 13. The ignition process is not calculated in this simulation. It is assumed that the dynamic regression process occurs after ignition. The results of the initial moment are obtained by the steady-state simulation. Then, the dynamic simulation was carried out on this basis. The combustion products of Al are mainly Al_2O_3, and the mass fraction of Al_2O_3 along the axial distance gradually increases. In the nozzle outlet, Al_2O_3 is carried out by the combustion chamber gas. The distribution of C_4H_6 is similar to Al_2O_3. The average mass fraction of Al_2O_3 and C_4H_6 are 0.262 and 0.087, respectively. The average mass fraction of O_2 and H_2O are 0.182 and 0.384, respectively, and the average mass fraction of H_2O is higher than other species. It is noticed that a little O_2 is ejected through the nozzle of this HRM, and the incomplete combustion occurs in the inner flow field. Therefore, the efficiency of the hybrid rocket motor decreases.

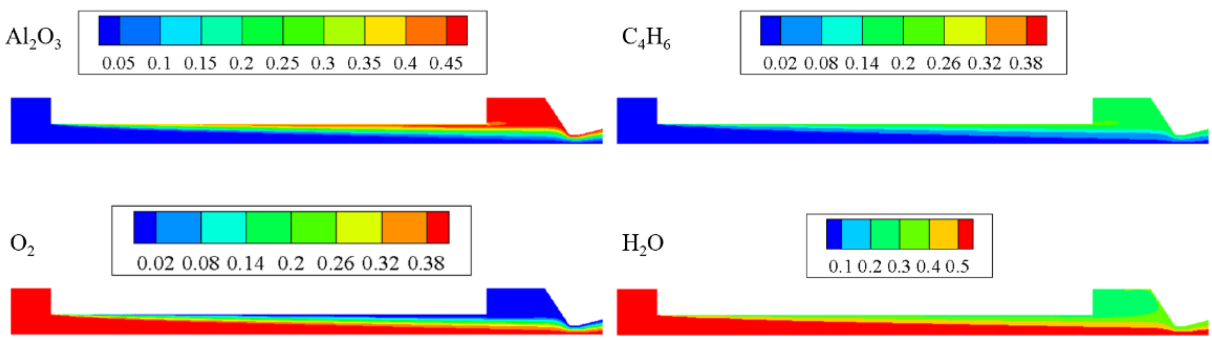

Figure 13. Mass fraction of four species in this HRM.

4.2. Verification of Firing Test

The photograph of the firing test in this HRM is shown in Figure 14. A large number of metal particles are ejected in the tail flame. The results demonstrate that when the content of Al is high, Al particles cannot fully react in the combustion chamber, because some Al particles are carried out by combustion chamber gas. At the same time, it can be obtained that the operating environment of the nozzle in this motor is very serious, therefore, an obvious ablation appears on the throat of the nozzle. Comparing the change in nozzle throat diameter before and after the test, it is found that the nozzle ablation rate is 0.16 mm/s. According to ref. [22], the nozzle ablation rate without Al is 0.05 mm/s. Therefore, a better ablation resistance material is required for Al-containing fuels in HRMs, such as copper-infiltrated tungsten materials.

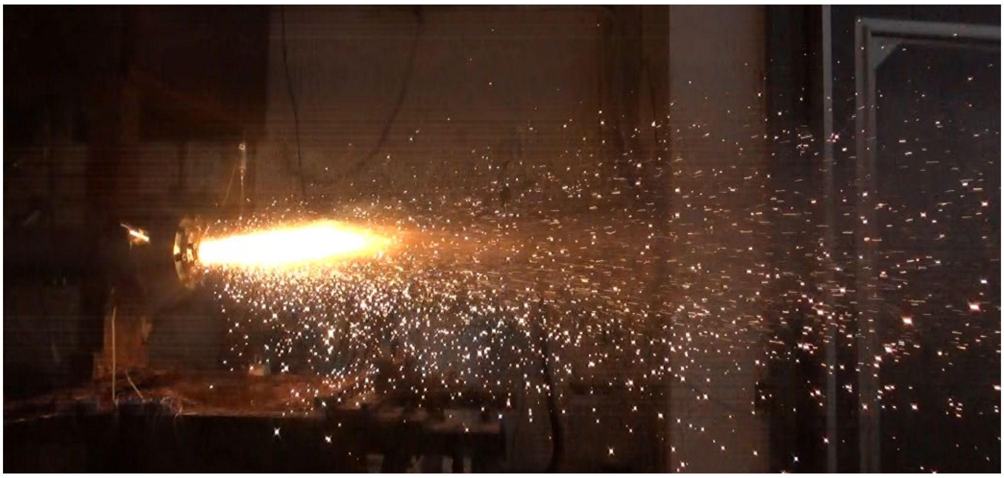

Figure 14. Photograph of the firing test.

In addition, the results of the firing test and simulation are represented in Figure 15. F refers to the thrust and m_o refers to the mass flow rate of the oxidizer. To ensure the safety of the ground experiment, reducing the delay time of catalytic decomposition, five pulses are used. A short-time flow feed of oxidizer is defined as the pulse, which lasts for 100 ms. GN_2 blowing was adopted to remove hydrogen peroxide after the test. The results show that the average oxidizer mass flow rate is 160 g/s in the firing test, and the average thrust reached 450 N, which was smooth during the operation process. The average thrust is 434.8 N in the simulation, which is only 3.4% in error with the test. The thrust of this simulation gradually increased during the operation process. The main reason is that the increase of the combustion surface area will weaken the effect of reduced regression rate. When the mass flow rate of the oxidizer is constant, the regression rate will decrease with time, as shown in Figure 16. In 0–1.5 s, the slope of regression rate decreasing is large, which is because the regression rate is high within this period. The port area increases rapidly with the regression of grain surface. Therefore, the mass flux of oxidizer reduces rapidly, resulting in a rapid decrease of regression rate. In 1.5–5.5 s, the slope of the regression rate decreases gradually. The main reason is that the regression rate is lower than 0–1.5 s. In 5.5–9 s, the slope of regression rate decreasing further decreases, which is because the regression rate has decreased obviously compared with the regression rate at the initial moment. The port area increases more slowly, resulting in a further decrease in the slope of regression rate reduction. The average regression rate of the hybrid rocket motor in the simulation is 0.854 mm/s. In the ground firing test, the average regression rate of the hybrid rocket motor obtained by the instantaneous regression rate analysis method [18] is 0.944 mm/s. The pure HTPB regression rate was calculated to be 0.50 mm/s for the same oxidizer mass flow rate according to reference [22], thus, the addition of 58% Al enhanced the regression rate of the HRMs by 88.8%. The results show that the addition of Al can significantly increase the regression rate of HRMs.

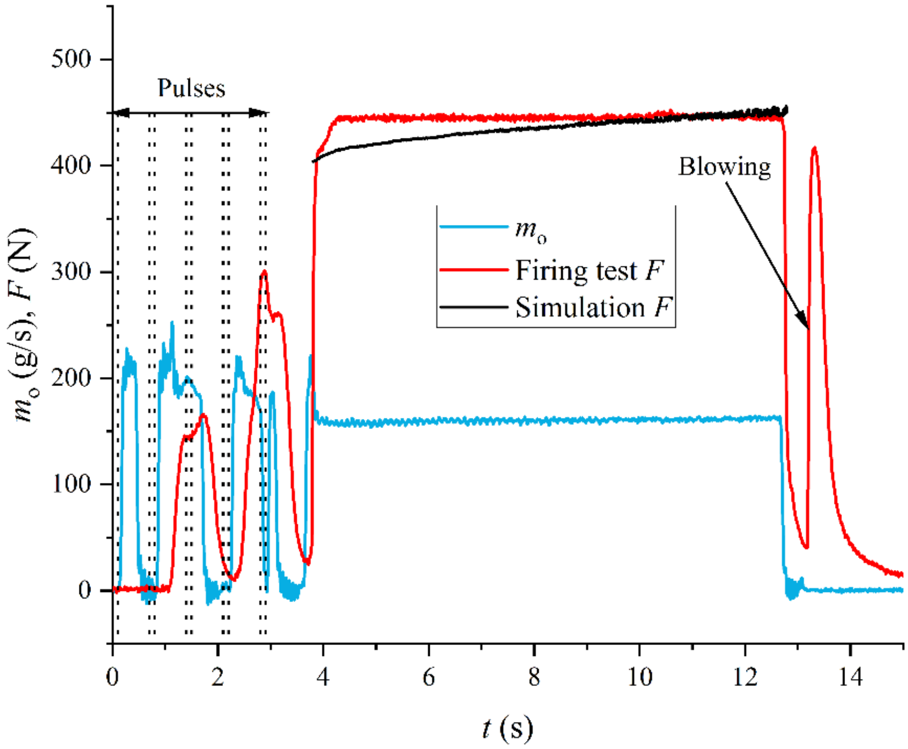

Figure 15. The results of the firing test and simulation.

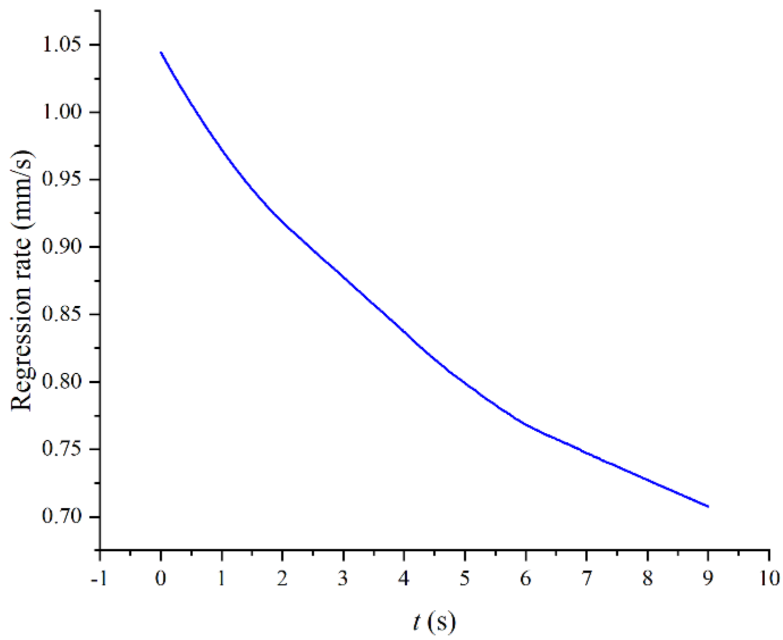

Figure 16. The regression rate of this HRM with time.

The results of the firing test and numerical simulation are shown in Table 3. In the firing test, the average pressure is 1.68 MPa, and the pressure of the simulation is 1.704 MPa. The error of test and simulation is 1.4%. It is indicated that the simulation model is relatively accurate. The deviation of the characteristic velocity and specific impulse between test and simulation are 2.9% and 0.9%, respectively. This investigation provides a valuable reference for HRMs design and simulation.

Table 3. Results of firing test and numerical simulation.

Parameter	Firing Test	Simulation	Error/%
Combustion chamber pressure (MPa)	1.680	1.704	1.4
Regression rate (mm/s)	0.944	0.854	9.5
Characteristic velocity (m/s)	1446.8	1404.3	2.9
Specific impulse (s)	204.99	206.91	0.9

5. Conclusions

In this study, the dynamic numerical simulation model of HRMs with Al-containing fuel is established, combined with the realizable k-ε model, fuel pyrolysis model, finite-rate chemical reaction models, and dynamic mesh technology. The effect of Al on the performance of HRMs such as regression rate is obtained. In addition, ground firing tests were carried out to verify the simulation model based on the lab-scale HRMs. It is noted that Al particle diameter is 2 μm in this investigation. The main conclusions are as follows:

(1) The use of dynamic mesh technology to simulate the combustion surface regression of HRMs containing Al fuel has obvious advantages. Compared with the ground firing test, the errors of average thrust and combustion chamber pressure are 3.4% and 1.4%, respectively, indicating that this investigation can make the numerical simulation closer to the firing test results.

(2) The dynamic simulation shows that with the continuous regression of the combustion surface, the vortex of the pre-chamber is divided into two vortices from one main vortex, in which the vortex near the front of the grain will make the regression rate downstream increase.

(3) The results show that the addition of Al can obviously increase the regression rate of HRMs. The addition of 58% Al enhanced the regression rate by 88.8% compared with pure HTPB.

(4) The Al-containing fuel obviously enhances the ablation of the nozzle, which reaches 0.16 mm/s due to the higher combustion temperature and the scouring of the metal particles, therefore, a better ablation resistance material is required for Al-containing fuel in HRMs.

In the author's opinion, radiation or large eddy models can be considered in the future to improve the numerical simulation accuracy. In addition, the 3D dynamic simulation of hybrid rocket motor is also necessary to make the model more adaptable. When the simulation accuracy is higher, the thrust of hybrid rocket motor can be predicted more accurately so as to achieve more accurate thrust control.

Author Contributions: Conceptualization, H.T. and X.M.; methodology, X.M.; software, X.M.; validation, H.Z., C.L. and L.H.; formal analysis, X.M.; investigation, H.Z.; resources, H.T. and G.C.; data curation, X.M.; writing—original draft preparation, X.M.; writing—review and editing, H.T.; visualization, H.Z.; supervision, H.T.; project administration, H.T.; funding acquisition, H.T and G.C. All authors have read and agreed to the published version of the manuscript.

Funding: This research was funded by the National Natural Science Foundation of China, grant number U20B2034.

Acknowledgments: The authors would like to express their gratitude to Beihang University, who supported the hybrid technology development.

Conflicts of Interest: The authors declare no conflict of interest.

Nomenclature

Variables	
Φ	general variable
Γ	generalized diffusion coefficient
S_Φ	source item
ρ	density
t	time
x	axial coordinates
r	radial coordinates
u	axial velocities
v	radial velocities
k	turbulence energy coefficient
ε	turbulence dissipation rate
λ_g	thermal conductivity of gas products
h_g	enthalpy of fuel pyrolysis products at fuel surface
h_s	enthalpy of solid fuel at initial temperature
ρ_f	density of solid fuel
ρ_g	density of pyrolysis products
$\dot{r}$	the fuel regression rate
T_s	temperature of the solid fuel combustion surface
A	Arrhenius pre-exponential constant
E_a	Arrhenius activation energy
R	universal molar gas constant
A_1	constant in the chemical model
B	constant in the chemical model
E	chemical activation energy
Abbreviations	
HRM	Hybrid Rocket Motor
HTPB	Hydroxy-terminated Polybutadiene
PLC	Programmable Logic Controller
HP	Hydrogen Peroxide
RPA	Rocket Propulsion Analysis
GN_2	Gas Nitrogen

References

1. Di Martino, G.D.; Carmicino, C.; Mungiguerra, S.; Savino, R. The Application of Computational Thermo-Fluid-Dynamics to the Simulation of Hybrid Rocket Internal Ballistics with Classical or Liquefying Fuels: A Review. *Aerospace* **2019**, *6*, 56. [CrossRef]
2. Bhadran, A.; Manathara, J.G.; Ramakrishna, P.A. Thrust Control of Lab-Scale Hybrid Rocket Motor with Wax-Aluminum Fuel and Air as Oxidizer. *Aerospace* **2022**, *9*, 56. [CrossRef]
3. Kara, O.; Karakaş, H.; Karabeyoğlu, M.A. Hybrid Rockets with Mixed N2O/CO2 Oxidizers for Mars Ascent Vehicles. *Acta Astronaut.* **2020**, *175*, 254–267. [CrossRef]
4. Meng, X.; Tian, H.; Zhu, H.; Wang, Z.; Yu, R.; Guo, Z.; Cai, G. Effects of Aluminum and Aluminum Hydride Additives on the Performance of Hybrid Rocket Motors Based on 95% Hydrogen Peroxide. *Aerosp. Sci. Technol.* **2022**, *130*, 107914. [CrossRef]
5. Tian, H.; Meng, X.; Zhu, H.; Li, C.; Yu, R.; Zhang, Y.; Cai, G. Dynamic Characteristics Study of Regression Rate in Variable Thrust Hybrid Rocket Motor. *Acta Astronaut.* **2022**, *193*, 221–229. [CrossRef]
6. Leccese, G.; Bianchi, D.; Nasuti, F.; Stober, K.J.; Narsai, P.; Cantwell, B. Simulations of Paraffin-Based Hybrid Rocket Engines and Comparison with Experiments. In Proceedings of the 53rd AIAA/SAE/ASEE Joint Propulsion Conference, Atlanta, GA, USA, 10–12 July 2017.
7. Migliorino, M.T.; Bianchi, D.; Nasuti, F. Numerical Simulations of the Internal Ballistics of Paraffin–Oxygen Hybrid Rockets at Different Scales. *Aerospace* **2021**, *8*, 213. [CrossRef]
8. Chiaverini, M.J.; Kuo, K.K.; Peretz, A.; Harting, G.C. Regression-Rate and Heat-Transfer Correlations for Hybrid Rocket Combustion. *J. Propuls. Power* **2001**, *17*, 99–110. [CrossRef]
9. Wei, C.; Pineda, D.I.; Paxton, L.; Egolfopoulos, F.N.; Spearrin, R.M. Mid-Infrared Laser Absorption Tomography for Quantitative 2D Thermochemistry Measurements in Premixed Jet Flames. *Appl. Phys. B Lasers Opt.* **2018**, *124*, 123. [CrossRef]
10. Goldenstein, C.S.; Schultz, I.A.; Spearrin, R.M.; Jeffries, J.B.; Hanson, R.K. Scanned-Wavelength-Modulation Spectroscopy near 2.5 Mm for H 2O and Temperature in a Hydrocarbon-Fueled Scramjet Combustor. *Appl. Phys. B Lasers Opt.* **2014**, *116*, 717–727. [CrossRef]

11. Li, F.; Yu, X.; Gu, H.; Li, Z.; Zhao, Y.; Ma, L.; Chen, L.; Chang, X. Simultaneous Measurements of Multiple Flow Parameters for Scramjet Characterization Using Tunable Diode-Laser Sensors. *Appl. Opt.* **2011**, *50*, 6697–6707. [CrossRef] [PubMed]
12. Casalino, L.; Masseni, F.; Pastrone, D. Optimal Design of Electrically Fed Hybrid Mars Ascent Vehicle. *Aerospace* **2021**, *8*, 181. [CrossRef]
13. Casalino, L.; Masseni, F.; Pastrone, D. Hybrid Rocket Engine Design Optimization at Politecnico Di Torino: A Review. *Aerospace* **2021**, *8*, 226. [CrossRef]
14. George, P.; Krishnan, S.; Varkey, P.; Ravindran, M.; Ramachandran, L. Fuel Regression Rate Enhancement Studies in HTPB/GOX Hybrid Rocket Motors. In Proceedings of the 34th AIAA/ASME/SAE/ASEE Joint Propulsion Conference and Exhibit, Cleveland, OH, USA, 13–15 July 1998; American Institute of Aeronautics and Astronautics: Reston, VA, USA, 1998.
15. Sun, X.; Tian, H.; Li, Y.; Yu, N.; Cai, G. Regression Rate Behaviors of HTPB-Based Propellant Combinations for Hybrid Rocket Motor. *Acta Astronaut.* **2016**, *119*, 137–146. [CrossRef]
16. Sun, X.; Tian, H.; Yu, N.; Cai, G. Regression Rate and Combustion Performance Investigation of Aluminum Metallized HTPB/98HP Hybrid Rocket Motor with Numerical Simulation. *Aerosp. Sci. Technol.* **2015**, *42*, 287–296. [CrossRef]
17. Strand, L.D.; Ray, R.L.; Anderson, F.A.; Cohen, N.S. Hybrid Rocket Fuel Combustion and Regression Rate Study. In Proceedings of the 28th Joint Propulsion Conference and Exhibit, Nashville, TN, USA, 6–8 July 1992. [CrossRef]
18. Li, X.; Zeng, P.; Tian, H.; Cai, G. Instantaneous Fuel Regression Rate Analysis of Hybrid Rocket Motor Experiment. *J. Propuls. Technol.* **2012**, *33*, 5.
19. Available online: https://www.rocket-propulsion.com/index.htm (accessed on 1 January 2021).
20. Cheng, G.; Farmer, R.; Jones, H.; McFarlane, J. Numerical Simulation of the Internal Ballistics of a Hybrid Rocket Motor. In Proceedings of the 32nd Aerospace Sciences Meeting and Exhibit, Reno, NV, USA, 10–13 January 1994. [CrossRef]
21. Zhang, S.; Hu, F.; Wang, D.; Okolo, N.P.; Zhang, W. Numerical Simulations on Unsteady Operation Processes of N2O/HTPB Hybrid Rocket Motor with/without Diaphragm. *Acta Astronaut.* **2017**, *136*, 115–124. [CrossRef]
22. Farbar, E.; Louwers, J.; Kaya, T. Investigation of Metallized and Nonmetallized Hydroxyl Terminated Polybutadiene/Hydrogen Peroxide Hybrid Rockets. *J. Propuls. Power* **2007**, *23*, 476–486. [CrossRef]